View Article Online / Journal Homepage / Table of Contents for this issue
Dynamic Article Links

Dalton Transactions

Cite this: *Dalton Trans.*, 2012, **41**, 13496

www.rsc.org/dalton

PAPER

Published on 10 September 2012. Downloaded by University of Texas Libraries on 19/08/2016 18:44:00.

Chemical vapour deposition of amorphous Ru(P) thin films from Ru trialkylphosphite hydride complexes†

W. Jeffrey McCarty, Xiaoping Yang, Lauren J. DePue Anderson and Richard A. Jones*

Received 12th July 2012, Accepted 8th September 2012
DOI: 10.1039/c2dt31541f

The ruthenium phosphite hydride complexes $H_2Ru(P(OR)_3)_4$ (R = Me (**1**), Et (**2**), ^{i}Pr (**3**)) were used as CVD precursors for the deposition of films of amorphous ruthenium–phosphorus alloys. The as-deposited films were X-ray amorphous and XPS analysis revealed that they were predominantly comprised of Ru and P in zero oxidation states. XPS analysis also showed the presence of small amounts of oxidized ruthenium and phosphorus. The composition of the films was found to depend on ligand chemistry as well as the deposition conditions. The use of H_2 as the carrier gas had the effect of increasing the relative concentrations of P and O for all films. Annealing films to 700 °C under vacuum produced films of polycrystalline hcp Ru while a flowing stream of H_2 resulted in polycrystalline hcp RuP.

Introduction

The replacement of aluminum with copper as an interconnect metal in microelectronic devices in the late 1980's brought a new set of fabrication challenges that led to significant long-term changes in semiconductor manufacturing processes. A key problem associated with copper as an interconnect material is its ability to electromigrate through the inter-layer dielectric, thus degrading device performance.[1] This issue can be addressed by the inclusion of an interstitial layer of a material between the copper and dielectric that acts as a diffusion barrier and prevents intermixing. Ideal materials for this role exhibit low resistivity, high thermal stability and good adhesion to both copper and silicon. There is considerable interest in early transition metal nitrides such as TiN, HfN and ZrN as barriers, while TaN in particular has become widely used commercially.[2] One drawback with the use of TaN, however, is the requirement of successive layers of PVD-grown TaN, Ta and Cu for the complete formation of the barrier layer. Thus the potential of this multilayer solution may be limited as the ever-decreasing feature sizes of integrated circuit components will require thinner and more conformal diffusion barriers.

Ruthenium is a viable alternative to TaN based diffusion barriers due to its high conductivity and chemical inactivity with copper and silicon.[3] Furthermore films of Ru adhere well to silicon and can be directly electroplated with copper.[4] However, ruthenium films tend to grow with columnar crystalline domains oriented perpendicular to the film surface, presenting efficient paths for copper migration.[5] Use of amorphous thin films as barrier layers would eliminate problems associated with grain boundary or stacking fault formation, as amorphous materials exhibit no long range order. Control over microstructure of deposited films leading to microcrystalline or amorphous films may improve the diffusion barrier properties.

Previous studies performed in these laboratories, with the single source CVD precursor *cis*-$H_2Ru(PMe_3)_4$, revealed a strong dependence on film morphology with precursor chemistry.[6] Thin films of Ru grown from this precursor show phosphorus incorporation in amounts of up to 20 atom% due to decomposition of PMe_3 ligands in the precursor. Furthermore, heteroatom incorporation is believed to interfere with crystallite formation, since the as-deposited films are X-ray amorphous, showing no long range order. X-ray photoelectron spectroscopy (XPS) studies revealed information about the chemical states of the elements within the film, and support the formulation of a Ru(P) alloy in which both Ru and P are in a formally zero oxidation state.

As an extension of the results obtained previously, a series of ruthenium hydride complexes were synthesized with various phosphorus donor ligands for use as single source CVD precursors. Coordination complexes incorporating trialkylphosphite ($P(OR)_3$) ligands with several different R-groups were studied in order to determine the possible effects of precursor ligand chemistry on film morphology and composition. Trialkylphosphite ligands were chosen as the P donor ligands for the precursor complexes since they are generally more air stable and less expensive than corresponding trialkylphosphines. Furthermore thermal decomposition pathways of phosphites have been shown to be similar to those of phosphines,[7] affording the possibility of control over the amount of P incorporation into films deposited from precursors utilizing these ligands.

Department of Chemistry and Biochemistry, The University of Texas at Austin, Welch Hall 2.204, 105 E. 24th St. STOP A5300, Austin, Texas, 78712-1224, USA. E-mail: rajones@mail.utexas.edu; Tel: +1 (512) 471-1706

† CCDC 888775–888777. For crystallographic data in CIF or other electronic format see DOI: 10.1039/c2dt31541f

 This journal is © The Royal Society of Chemistry 2012

View Article Online

Published on 10 September 2012. Downloaded by University of Texas Libraries on 19/08/2016 18:44:00.

Results and discussion

The *cis*-ruthenium hydride complexes $H_2Ru(P(OR)_3)_4$ (R = Me (**1**), Et (**2**), ^{i}Pr (**3**)) were reported by Muetterties and co-workers more than 30 years ago but were not structurally characterized.[8] In the present work, the complexes were synthesized by a slight modification of the method previously reported. The crude products consisted of flaky off-white solids that were purified by sublimation under reduced pressure (10^{-2} Torr). X-ray quality crystals of complexes **1** and **2** were grown by cooling hexane–methanol solutions to −30 °C. Similar recrystallization attempts for **3** led only to microcrystalline powders and although large colorless crystals were obtained by slow heating under vacuum in a zone sublimator they were not suitable for X-ray crystallography. The identities of **1–3** were confirmed by comparison of NMR and IR spectral data with that previously reported.[8]

The crystal structure of **1** is shown in Fig. 1 and selected bond lengths and angles are presented in Table 1. Crystallographic details are listed in Table 2. The complex crystallizes in the triclinic space group $P\bar{1}$ with six molecules per unit cell. The central Ru ion of the complex is six-coordinate with a *cis*-configuration of the hydride ligands. The hydride hydrogen atoms were located as peaks in reasonable locations on a difference Fourier map and included without refinement. The position of the hydride ligands is further established by the approximate see-saw molecular geometry formed by the four trimethylphosphite ligands. The two P atoms of the mutually *trans* phosphite ligands form an angle of *ca.* 155.30° at Ru, while the other two $P(OMe)_3$ ligands form a mutual angle of 96.25°, leaving room for the coordination of the relatively small hydride ligands.

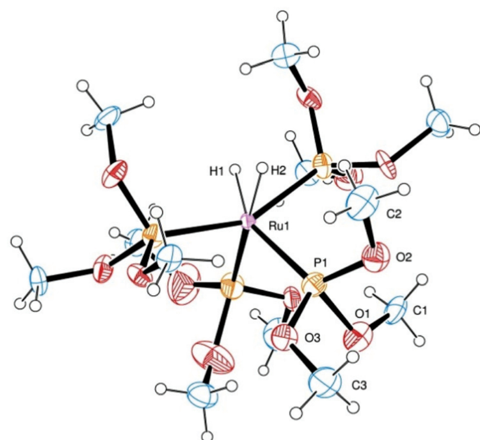

Fig. 1 ORTEP diagram and partial atom numbering scheme of *cis*-$H_2Ru(P(OMe)_3)_4$ (**1**). Thermal ellipsoids are drawn at the 30% probability level.

Table 1 Selected bond lengths [Å] and angles [°] for **1**

Ru(1)–P(2)	2.257(3)	Ru(1)–P(1)	2.269(3)
Ru(1)–P(3)	2.273(3)	Ru(1)–P(4)	2.279(3)
P(2)–Ru(1)–P(1)	101.86(11)	P(2)–Ru(1)–P(3)	155.31(10)
P(1)–Ru(1)–P(3)	95.62(11)	P(2)–Ru(1)–P(4)	96.75(10)
P(1)–Ru(1)–P(4)	96.24(12)	P(3)–Ru(1)–P(4)	98.55(11)

Table 2 Crystallographic details and refinement data for **1**, **2** and **4**

	1	**2**	**4**
Empirical formula	$C_{12}H_{38}O_{12}P_4Ru$	$C_{24}H_{62}O_{12}P_4Ru$	$C_{12}H_{36}Cl_2O_{12}P_4Ru$
Formula weight	599.37	767.69	668.26
Temperature	153(1) K	153(1) K	100(1) K
Wavelength	0.71073 Å	0.71073 Å	0.71073 Å
Crystal system	Triclinic	Triclinic	Monoclinic
Space group	$P\bar{1}$	$P\bar{1}$	$P2_1/n$
Unit cell dimensions	a = 10.000(5) Å	a = 11.465(2) Å	a = 18.310(4) Å
	b = 19.007(5) Å	b = 18.064(4) Å	b = 20.351(4) Å
	c = 20.695(4) Å	c = 18.784(4) Å	c = 28.915(6) Å
	α = 78.840(5)°	α = 100.57(3)°	α = 90°
	β = 87.286(6)°	β = 99.47(3)°	β = 90.03(3)°
	γ = 79.763(5)°	γ = 96.97(3)°	γ = 90°
Volume	3797(2) Å^3	3725.7(13) Å^3	10775(4) Å^3
Z	6	4	16
Density (calculated)	1.573 mg m^{-3}	1.369 mg m^{-3}	1.648 mg m^{-3}
Absorption coefficient	0.921 mm^{-1}	0.643 mm^{-1}	1.067 mm^{-1}
F(000)	1860	1624	5472
Theta range for data collection	3.01 to 25.00°	1.44 to 25.00°	2.99 to 25.00°
Reflections collected	22 826	21 350	18 957
Independent reflections	22 826 [R(int) = 0.0273]	12 350 [R(int) = 0.0490]	18 957 [R(int) = 0.000]
Data/restraints/parameters	13 281/540/784	13 004/599/858	18 957/744/1117
Goodness-of-fit on F^2	1.069	1.020	1.240
Final R^a indices [$I > 2\sigma(I)$]	R_1 = 0.0852	R_1 = 0.0967	R_1 = 0.0723
	wR_2 = 0.2314	wR_2 = 0.2215	wR_2 = 0.1287
R^a indices (all data)	R_1 = 0.1137	R_1 = 0.1559	R_1 = 0.0791
	wR_2 = 0.2479	wR_2 = 0.2489	wR_2 = 0.1316
Largest diff. peak and hole	3.173 and −1.310 e Å^{-3}	3.300 and −1.527 e Å^{-3}	1.649 and −0.976 e Å^{-3}

^{a} $R_1 = \Sigma_{hkl}(|F_o| - |F_c|)/\Sigma_{hkl}|F_o|$; $wR_2 = [\Sigma w(|F_o| - |F_c|)^2/\Sigma w|F_o|^2]^{1/2}$.

Published on 10 September 2012. Downloaded by University of Texas Libraries on 19/08/2016 18:44:00.

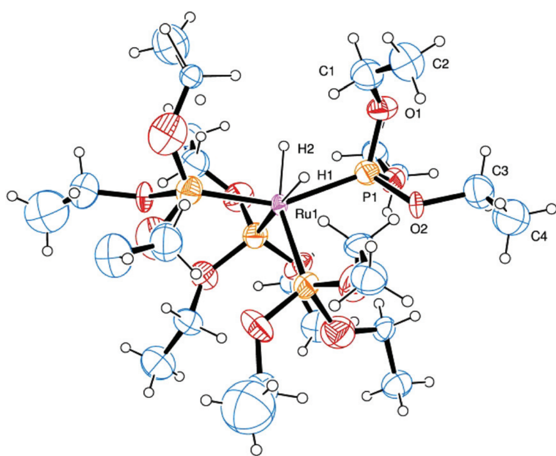

Fig. 2 ORTEP diagram and partial atom numbering scheme of *cis*-$H_2Ru(P(OEt)_3)_4$ (**2**). Thermal ellipsoids are drawn at the 30% probability level.

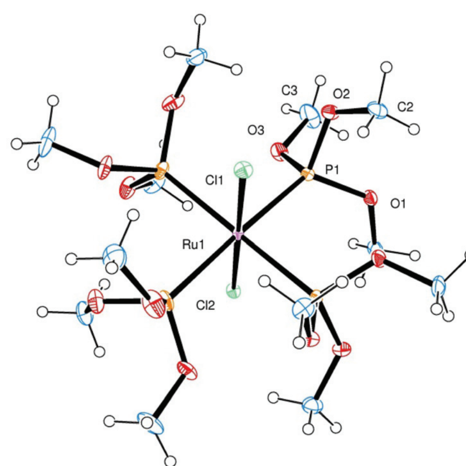

Fig. 3 ORTEP diagram and partial atom numbering scheme of $Cl_2Ru(P(OMe)_3)_4$ (**4**). Thermal ellipsoids are drawn at the 30% probability level.

Table 3 Selected bond lengths [Å] and angles [°] for **2**

Ru(1)–P(3)	2.255(3)	Ru(1)–P(2)	2.259(3)
Ru(1)–P(1)	2.272(3)	Ru(1)–P(4)	2.278(3)
P(3)–Ru(1)–P(2)	152.03(11)	P(3)–Ru(1)–P(1)	101.32(10)
P(2)–Ru(1)–P(1)	96.59(10)	P(3)–Ru(1)–P(4)	96.19(10)
P(2)–Ru(1)–P(4)	102.58(10)	P(1)–Ru(1)–P(4)	97.56(10)

Table 4 Selected bond lengths [Å] and angles [°] for **4**

Ru(1)–P(2)	2.3304(16)	Ru(1)–P(1)	2.3380(16)
Ru(1)–P(3)	2.3390(16)	Ru(1)–P(4)	2.3457(16)
Ru(1)–Cl(2)	2.4331(15)	Ru(1)–Cl(1)	2.4473(15)
P(2)–Ru(1)–P(1)	89.65(6)	P(2)–Ru(1)–P(3)	90.14(6)
P(1)–Ru(1)–P(3)	173.52(6)	P(2)–Ru(1)–P(4)	174.66(6)
P(1)–Ru(1)–P(4)	88.40(6)	P(3)–Ru(1)–P(4)	92.36(6)
P(2)–Ru(1)–Cl(2)	91.88(5)	P(1)–Ru(1)–Cl(2)	87.36(6)
P(3)–Ru(1)–Cl(2)	86.18(5)	P(4)–Ru(1)–Cl(2)	93.00(5)
P(2)–Ru(1)–Cl(1)	88.74(5)	P(1)–Ru(1)–Cl(1)	93.97(6)
P(3)–Ru(1)–Cl(1)	92.50(5)	P(4)–Ru(1)–Cl(1)	86.43(5)
Cl(2)–Ru(1)–Cl(1)	178.54(5)		

The two phosphite ligands coordinated *trans* to the hydrides exhibit a slightly shorter average Ru–P bond length (2.265 Å av. for Ru(1), 2.262 Å av. for Ru(2), 2.255 Å av. for Ru(3)) compared to the other two phosphite ligands (2.275 Å av. for Ru(1), 2.281 Å av. for Ru(2), 2.287 Å av. for Ru(3)), reflecting the *trans*-directing influence of the hydride ligands. Complex **2** was synthesized similarly to **1**, but using triethylphosphite as the phosphorus containing ligand. The crystal structure of **2** is shown in Fig. 2 and selected bond lengths and angles are presented in Table 3, while additional crystallographic details are summarized in Table 2. Complex **2** crystallizes in the triclinic space group $P\bar{1}$ with four independent molecules in the unit cell. The compound is isostructural with **1**, with the phosphite ligands arranged in a similar see-saw geometry about the central ruthenium ion and the hydride atoms located *cis* to each other. The P–Ru–P angle for the ligands *trans* to the hydrides (158.05°) is significantly larger than that for the ligands *cis* to the hydrides (97.57°). As in complex **1**, a slight *trans*-directing influence of the hydride ligands is observed for complex **2** ($Ru–P_{cis}$ = 2.75 Å, av.; $Ru–P_{trans}$ = 2.57 Å, av. for the $P(OEt)_3$ ligands *cis* and *trans* to the hydride atoms, respectively).

The complex *trans*-$Cl_2Ru(P(OMe)_3)_4$ (**4**) was isolated as an intermediate in the synthesis of **1**, and although the preparation and spectral characterization of this compound had been previously reported,[8] surprisingly, it had not been structurally characterized by single crystal X-ray diffraction. The complex is not suitable for use as a CVD precursor because of the two chloride ligands, but it may be possible to exchange these with other functional groups to give compounds which are appropriate for CVD applications.

Complex **4** crystallizes in the centrosymmetric space group $P2_1/n$ with four molecules per unit cell (Fig. 3). Two chloride ligands are coordinated to the central ruthenium atom in a *trans* configuration, giving the $RuCl_2P_4$ core virtual D_{4h} symmetry.

The average Ru–P distance of 2.338 Å is slightly longer than that found in complexes **1** and **2**, and is typical for ruthenium phosphite complexes (Table 4).[9] The angular separation of the phosphite ligands is approximately 90°, however they are not coplanar. The average *trans* P–Ru–P angle of 174.09(1)° results in a slight distortion of the four phosphite ligands from a square planar geometry which allows for steric relief of the bulky ligands. Infrared and NMR spectroscopic data for **4** are consistent with previously reported data.[8]

Thin film studies

Thin films were grown from complexes **1–3** at various temperatures in a horizontal hot-wall CVD reactor with ultra-high purity argon or hydrogen as the carrier gas. In a typical deposition, a saturator tube was charged with approximately 10–20 mg of sample and the gas flow rate was varied to allow for optimal film growth. Each precursor was heated to a temperature which was adequate to sufficiently volatilize the complex, while the deposition chamber was maintained at the lowest temperature in which deposition occurred. The sublimation and deposition temperatures were found to increase with precursor

 This journal is © The Royal Society of Chemistry 2012

View Article Online

molecular weight. A summary of deposition conditions and film compositions is presented in Table 5.

All deposited films appeared lustrous with a silver or golden hue and adhered well to the substrate (Si(100) with native oxide) as determined by the Scotch tape test. As shown in Fig. 4 for a typical film grown from **1**, scanning electron microscopy (SEM) revealed relatively smooth surfaces of uniform thickness (50–100 nm) and a lack of large crystalline grains. X-ray reflectivity measurements of selected films corroborate this range for film thickness. All of the as-deposited films were amorphous, as indicated by the lack of diffraction peaks present in the *ex situ* X-ray diffraction patterns taken immediately after film growth (Fig. 5). Compositional analysis of each film was performed by *ex-situ* X-ray photoelectron spectroscopy (XPS). Fig. 6 shows an XPS survey scan (top) and high resolution spectral regions (bottom) for a typical film grown from **2** at 400 °C under H_2. Peaks corresponding to Ru, P, O, and C were present in all films, with no traces of Cl impurities from the precursor synthesis.

Table 5 Summary of deposition conditions and film composition for Ru films. Film composition was determined by XPS

	Carrier gas (sccm)	Precursor temp. (°C)	Deposition temp. (°C)	Film composition (at.%)			
				Ru	P	O	C
1	Ar (10)	85	350	40	37	18	<5
1	H_2 (13)	85	350	23	27	48	<2
2	Ar (10)	110	400	51	31	16	<2
2	H_2 (10)	110	400	41	25	32	<2
3	H_2 (10)	120	420	34	21	42	<3

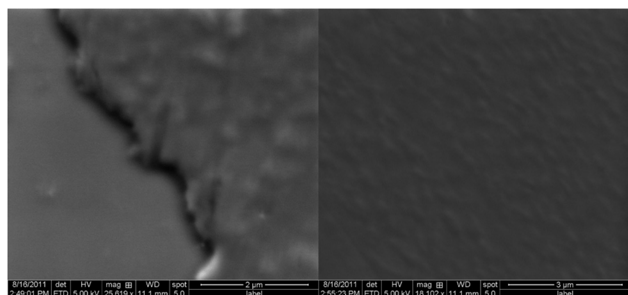

Fig. 4 SEM images of a typical film grown from **1** under H_2.

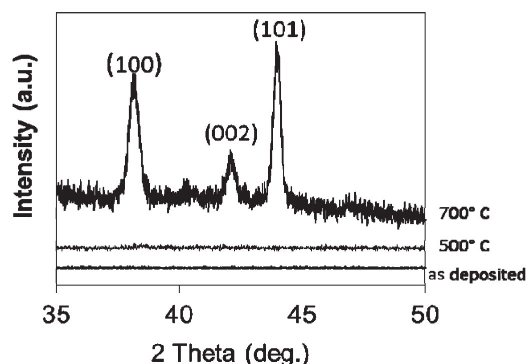

Fig. 5 XRD patterns of a typical hcp Ru film deposited from **2** under Ar and then annealed at various temperatures under dynamic vacuum.

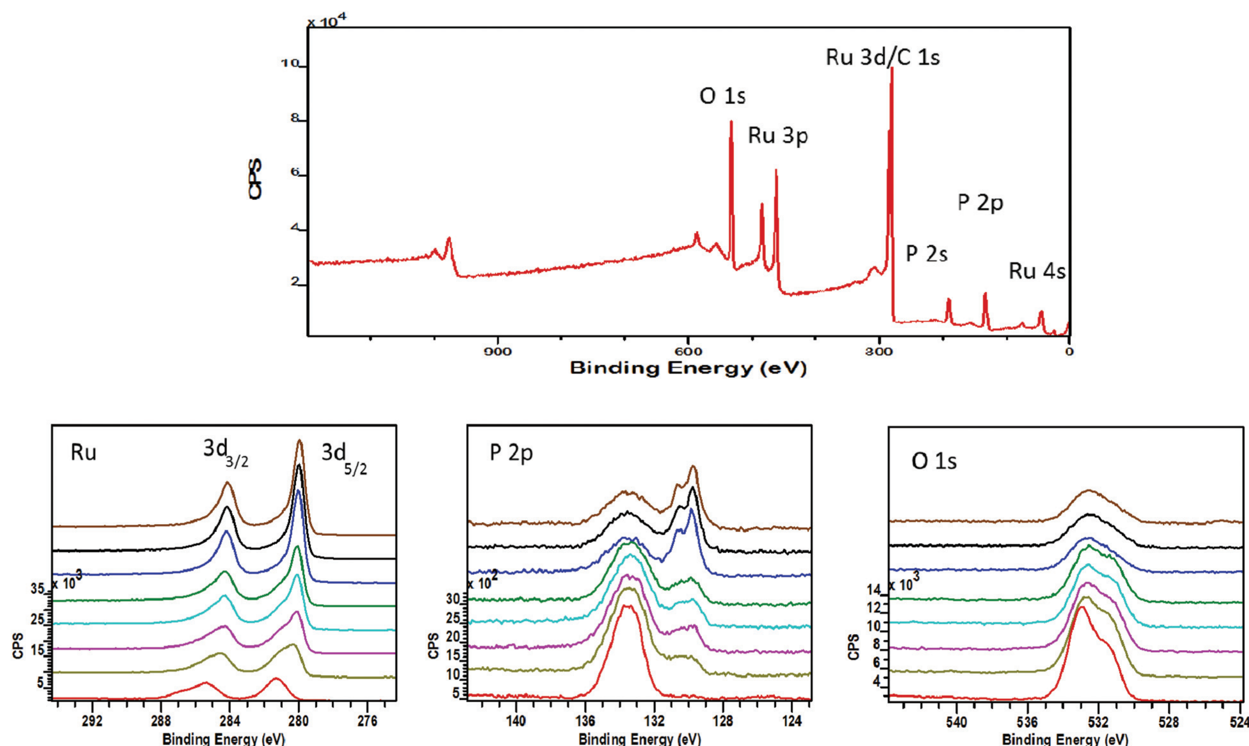

Fig. 6 XPS survey scan (top) of a typical film deposited from **2** at 400 °C under H_2. High resolution scans (bottom) for Ru, P, and O obtained from depth profiling. The bottom red scans correspond to the film surface, with sputtering ascending in 1 minute increments.

Published on 10 September 2012. Downloaded by University of Texas Libraries on 19/08/2016 18:44:00.

View Article Online

Published on 10 September 2012. Downloaded by University of Texas Libraries on 19/08/2016 18:44:00.

After brief (30 s) sputtering with Ar^+ to remove adventitious surface C and O contamination present from exposure to the atmosphere, the nature of the chemical states of the elements of interest were probed in more detail from high resolution data. Peaks with binding energies (BE) of 280.1 eV and 284.3 eV were observed for all films and correspond to the 3d doublet for elemental Ru.[10a] These peaks were found to be slightly asymmetric for all films, with lower intensity shoulders appearing at higher BE for both peaks of the doublet. The shoulders are centered at BE 280.8 eV and 284.9 eV, which is within the range of literature values[10b] for the binding energy of the Ru 3d doublet in RuO_2 ($3d_{5/2}$ = 280.7–281.0 eV; $3d_{3/2}$ 284.9–285.2 eV). This indicates that the films contain ruthenium in two distinct chemical environments; *i.e.* zero valent Ru comprising the majority of the films as well as small contributions from oxidized Ru (possibly from RuO_2, $Ru(PO_4)$, *etc.*). Oxygen was present in varying amounts for all films, likely a result of ligand decomposition. At least two distinct chemical environments for O could be reasonably modeled with peak fitting, with broad peaks appearing at BE 532.8 eV and 531.4 eV. The chemical state of P was found to be similar to that observed in Ru(P) films previously deposited from *cis*-$H_2Ru(PMe_3)_4$.[8] Three phosphorus peaks were present in two distinct regions, with a well resolved doublet at lower BE corresponding to elemental phosphorus ($2p_{1/2}$ = 130.6 eV; $2p_{3/2}$ = 129.7 eV) as well as a broad, lower intensity peak centered at 133.4 eV corresponding to oxidized phosphorus. No maxima were observed at BE lower than 129.7 eV, indicating a lack of phosphidic phosphorus (P^{3-}) in the as-deposited film.

The carbon content was found to be low for all films despite relatively high P and O content. It should be noted that the C 1s primary photoelectron peak at 284.5 eV directly overlaps with the Ru $3d_{3/2}$ peak located at 284.3 eV, thus making direct measurement of C content very difficult. The Ru $3d_{5/2}$ peak, however, does not overlap with the C signal. Therefore carbon content was estimated by constraining the peak area of the Lorenzian–Gaussian curves used to fit the experimental Ru 3d doublet to a 3 : 2 ratio, which corresponds to the theoretical value for peak height due to spin–orbit interactions of d-electrons. Assuming that the Ru $3d_{5/2}$ signal is due only to Ru and that the C 1s peak only overlaps the Ru $3d_{3/2}$ peak, the difference in area of the curve fitting data and experimental data corresponds to the atomic percentage of carbon. For all films, the C content was estimated to be below 5 atom%.

XPS depth profiling revealed an uneven distribution of elements throughout the films. For all films, C and O content was greater near the film surface undoubtedly due to adventitious contamination resulting from exposure to the atmosphere. Gentle Ar^+ sputtering drastically lowered the presence of these elements. Further sputtering was continued in 30 s intervals for up to 3 minutes to investigate the atomic composition throughout the films. Oxygen content was observed to decrease while Ru and P content generally increased throughout the thickness of the films. Depth profiles also clearly display key differences in film composition due to differing deposition conditions as well as post-deposition thermal treatment. For example, the two depth profiles shown in Fig. 7 illustrate the difference in composition in two films grown from the same precursor (**1**) but under different deposition conditions (Ar carrier gas *vs.* H_2). In other CVD studies on thin films of Rh we had found that the use of H_2 reduced the levels of C and O impurities.[11] However, in the present study films grown under H_2 generally showed lower Ru content than films grown with the same precursor and at the same temperature with Ar as a carrier gas. A hydrogen saturated atmosphere may hinder reductive elimination of H_2 from the metal-hydride precursors, thus preventing the initial formation of an open coordination site for the metal to adsorb to the surface of the substrate. Difficulty in producing pure films of Ru with H_2 as a carrier gas has also been observed with β-diketonato and β-ketoiminato precursors.[12]

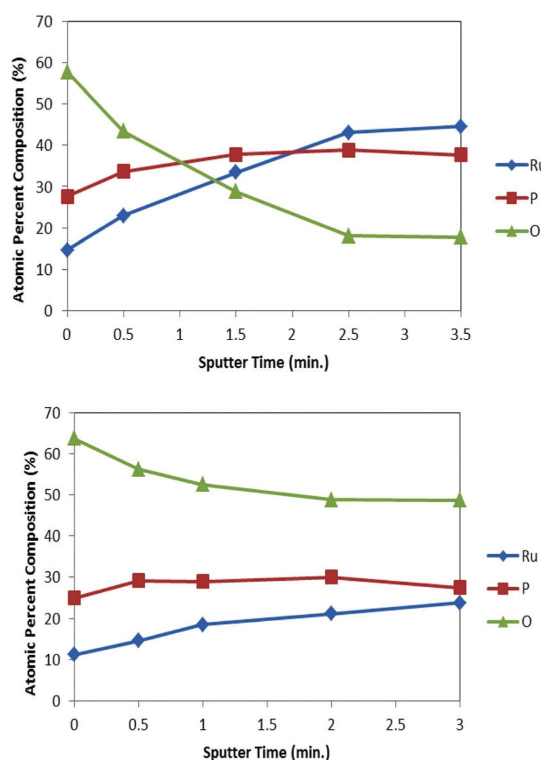

Fig. 7 XPS depth profiles of films deposited from **1** under Ar (top) and under H_2 (bottom).

Post-growth annealing experiments

The morphology as well as composition of the deposited films were found to vary depending on specific annealing conditions. The films remained amorphous upon heating to 500 °C for 3 h and then began to crystallize upon further heating to 700 °C. Films annealed under dynamic vacuum showed peaks at 2θ = 38.6, 42.4, and 44.2°, associated with the (100), (002), and (101) diffraction planes of hcp Ru respectively, indicating a microcrystalline morphology (Fig. 5). Crystallite size was estimated to be between 50 and 75 nm from the Scherrer equation using the two most intense reflections.[13] It should be noted that film strain as well as instrumental effects may also influence XRD peak broadening and is not accounted for using this equation, and thus the numbers presented represent a lower estimate of crystallite size. No diffraction peaks corresponding to crystalline phases of RuO_2 were detected for any film. Interestingly, thermal treatment of the films under flowing H_2 resulted in a change in film

 This journal is © The Royal Society of Chemistry 2012

View Article Online

Published on 10 September 2012. Downloaded by University of Texas Libraries on 19/08/2016 18:44:00.

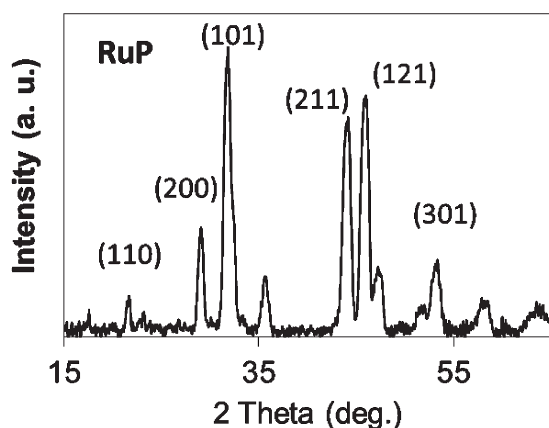

Fig. 8 XRD pattern of a typical RuP film deposited from **3** under H_2, followed by annealing under flowing H_2 at 700 °C.

composition along with an increase in particle size. A typical X-ray diffraction pattern of a film grown from **3** under H_2, and then annealed at 700 °C under flowing H_2 is presented in Fig. 8, and shows intense peaks corresponding to diffraction planes of polycrystalline hcp RuP (PDF #01-074-6494). The ability to control film composition as well as morphology by varying the thermal treatment conditions has potential for formation of a variety of binary phases of ruthenium phosphide – the chemical and electrical properties of which remain largely unexplored.

XPS depth profiling was used to compare the composition of pre- and post-annealed films. Fig. 9 shows depth profiles of a film deposited from **3** with H_2 as the carrier gas without annealing (top) and after annealing under flowing H_2 at 700 °C (bottom). The oxygen content throughout the thickness of the annealed film is substantially reduced after 3 minutes of Ar^+ sputtering, while the Ru : P ratio remains approximately constant at *ca.* 1.8 : 1. Changes in the chemical states of the elements due to the formation of RuP upon annealing were monitored by peak positions in the XPS spectra. A shift of 0.4 eV towards lower BE was observed for the P 2p doublet, indicating the formation of phosphidic P^{3-}, while the broad peak centered at 133 eV corresponding to oxidized phosphorus is not present in the annealed films. This is consistent with the drastic reduction in oxygen content in the H_2 annealed films. Interestingly, no apparent BE shift of the Ru 3d peak from Ru(0) to Ru(III) was observed upon annealing, though it should be noted that such a shift associated with formation of RuP may be small.

The films annealed under vacuum showed no visible change in morphology upon heating, while films annealed under flowing H_2 exhibited broad cracking features over the entire film, as shown in Fig. 10. This was accompanied by a darkening and loss of luster upon formation of crystalline RuP. Elemental mapping through energy dispersive X-ray spectroscopy (EDX) of the cracked films revealed an uneven distribution of Ru, P, O and Si across the surface of the films. As shown in Fig. 11, ruthenium and phosphorus are concentrated primarily within the deposited film, while silicon and oxygen signals arise mostly from the interstitial space between portions of the deposited film corresponding to the Si/SiO_2 substrate onto which the film was deposited. This anisotropic surface distribution of elements suggests that the Si and O content within the film is

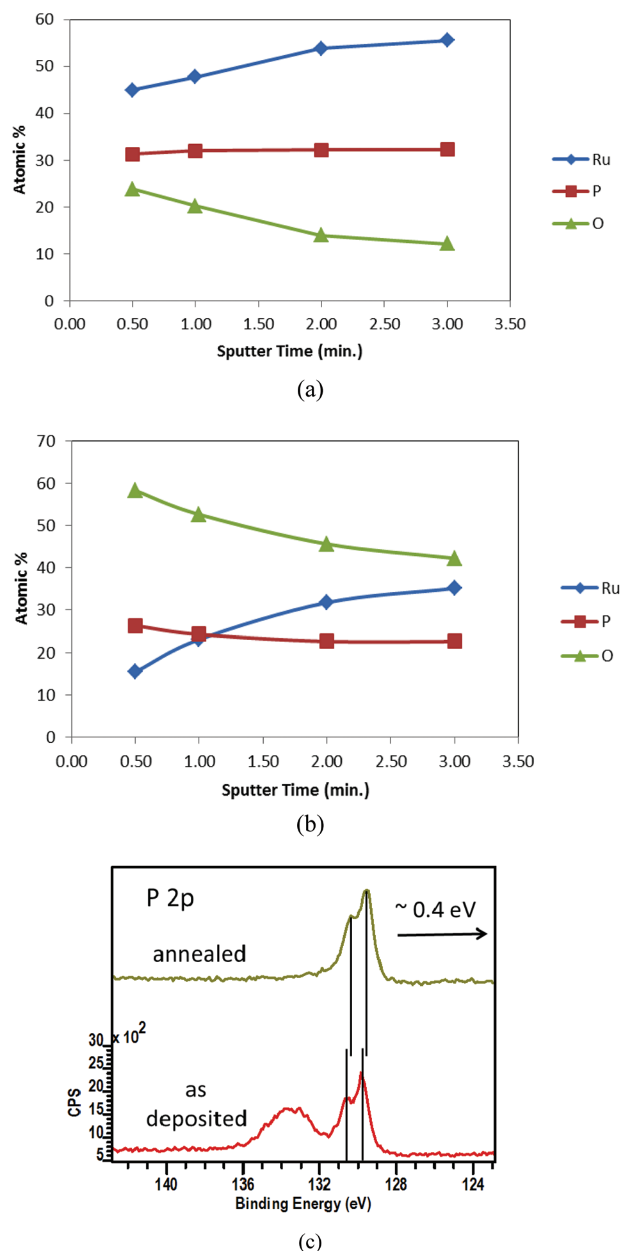

Fig. 9 XPS depth profiles (a and b) of films deposited from **3** under H_2. (a) As-deposited amorphous film, (b) film annealed at 700 °C in flowing H_2. (c) Illustrates the shift in BE (XPS) of the P 2p peak upon formation of RuP, and the disappearance of the broad peak corresponding to oxidized phosphorus that occurs upon annealing in H_2.

overestimated as determined by XPS, which has a spot size of approximately 300 × 700 μm.

Conclusions

Films of amorphous ruthenium–phosphorus alloys were grown by CVD using ruthenium phosphite hydride complexes as precursors. In all cases, the as-deposited films were X-ray amorphous and contained Ru and P in zero oxidation states. XPS analysis also revealed the presence of small amounts of oxidized ruthenium and phosphorus. The compositions of the films were

View Article Online

Published on 10 September 2012. Downloaded by University of Texas Libraries on 19/08/2016 18:44:00.

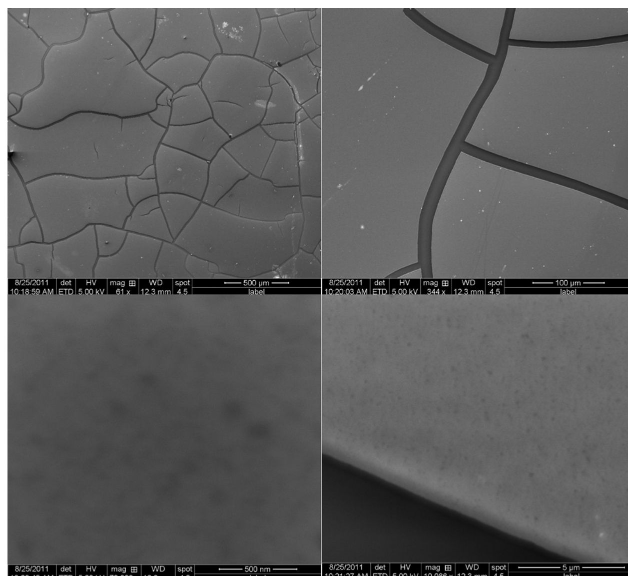

Fig. 10 SEM images of a typical film grown from **3** annealed under flowing H_2.

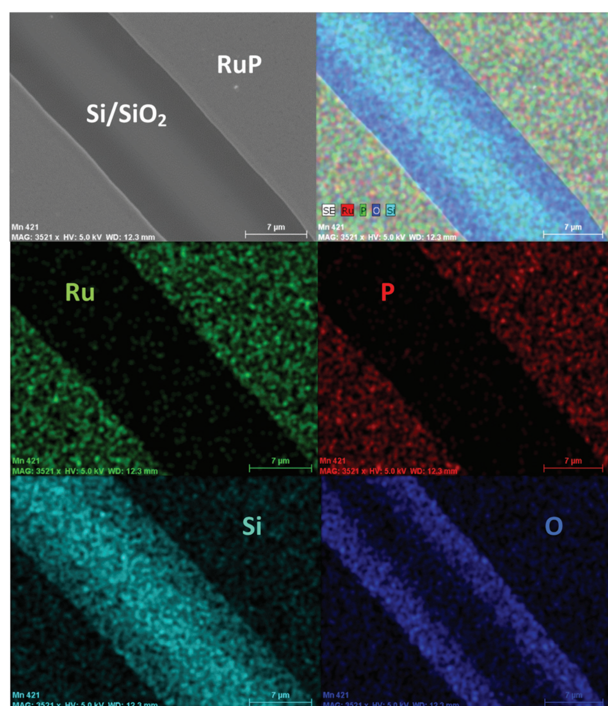

Fig. 11 EDX Quantitative Element Mapping of a typical film of Ru (P, O) annealed under flowing H_2 to give polycrystalline RuP, showing the relative locations of Ru, P, Si and O within the film. Ru and P are more concentrated in the thin film, while Si and O contributions primarily arise from the silicon substrate.

found to depend on ligand chemistry as well as deposition conditions. Films grown from $H_2Ru(P(OEt)_3)_4$ (**2**) generally showed higher Ru content. Surprisingly, the use of H_2 as a reactive carrier gas had the effect of increasing the relative concentration of P and O for all films. Further film growth studies are needed to optimize deposition conditions with these complexes, as well as elucidate the effects of morphology and composition on conductive properties of the resultant films. Additionally, detailed mechanistic studies would be helpful in helping to understand the chemical process by which both the Ru and P attain a zero oxidation state upon deposition.

Experimental

General procedures

Unless otherwise noted, all reactions were performed under a dry, oxygen-free nitrogen atmosphere or under vacuum using standard Schlenk line and dry box techniques. All solvents were dried prior to use by distillation from molten sodium or sodium benzophenoneketyl under nitrogen. The three phosphite complexes **1**, **2**, and **3** were prepared according to literature procedures.[8] Trimethylphosphite and triethylphosphite were purchased and used without further purification. Microanalyses (C,H,N) were performed by Galbraith Laboratories of Knoxville, TN or QTI Labs of Whitehouse, NJ. Melting points were determined in sealed capillaries under N_2 (1 atm.) on an Electrothermal Melting Point apparatus and are uncorrected. ESI mass spectra were collected on a Finnigan MAT TSQ 700 mass spectrometer. NMR spectra were recorded on a Varian 300 Unity Plus spectrometer (300 MHz at 298 K). Chemical shifts are referenced to the deuterated solvent. Infrared spectra were taken on a Nicolet IR 200 FTIR spectrometer between KBr plates.

Syntheses of *cis*-$H_2Ru(P(OR)_3)_4$; R = Me (1), Et (2), ^{i}Pr (3). The phosphite hydride complexes **1–3** were prepared using a modified literature procedure.[8] In a typical synthesis, a mixture of $RuCl_3 \cdot nH_2O$ (2.6 g, 0.010 mol) and $P(OR)_3$ (25 mL, excess) was stirred until the reaction subsided and the color turned red-brown. Sodium borohydride (2.0 g, 0.053 mol) was added and the mixture heated gently until the color turned off-white. Excess phosphite was then removed *in vacuo*. The residue was heated gently for 20 minutes in the presence of THF, ethanol, and $NaBH_4$ (3.0 g, 0.079 mol). The volatile products were removed under vacuum and the sticky residue was extracted into toluene (50 mL), and the mixture filtered. Evaporation of the filtrate led to an off-white solid, which was purified by sublimation (10^{-2} Torr) at temperatures between 120–160 °C for the three complexes. The recovered solids were then recrystallized from methanol (−30 °C) to yield large, colorless crystals. Yields typically ranged from 50 to 60%.

Synthesis of *trans*-$Cl_2Ru(P(OMe_3))_4$ (4). This complex was prepared using a modified literature procedure.[8] A mixture of $RuCl_3 \cdot nH_2O$ (0.26 g, 0.0010 mol) and trimethylphosphite (2.5 mL, excess) was stirred for 15 minutes. The solution turned dark red and evolved heat. Addition of $NaBH_4$ (1.0 g, 0.026 mol) in THF (50 mL) initiated a color change from red to brown to green. The heterogeneous solution was stirred for 45 minutes and then the solvent and excess trimethylphosphite were removed *in vacuo*. The yellow green residue was extracted into methylene chloride (100 mL) and then filtered. Solvent was removed *in vacuo* and the residue was extracted into hexane (100 mL) and the solution filtered. The yellow filtrate was

 This journal is © The Royal Society of Chemistry 2012

View Article Online

Published on 10 September 2012. Downloaded by University of Texas Libraries on 19/08/2016 18:44:00.

cooled to −30 °C and the resulting yellow crystals were collected and dried *in vacuo*. Isolated yield: 0.45 g, 70%.

Thin film growth

Films were grown in a horizontal, hot-wall CVD reactor consisting of a 2″ diameter Pyrex tube heated by a tube furnace. The precursor was heated in a saturator tube connected to the deposition assembly by VCR and Swagelok connections. Ultra high purity (99.999%) hydrogen or argon was used as the carrier gas at flow rates of 5–50 sccm controlled by a Fathom Technologies mass flow controller, with the overall pressure of the system maintained between 0.5 and 2 Torr. The temperature of the precursor was controlled by an oil bath, while the lines were heated separately with insulated heating tape. Films were grown on Si(100) wafers with native oxide cut into approximately 1 cm × 1 cm squares. The wafers were prepared by sequentially sonicating in hexane, isopropanol, and DI water, and then drying at 120 °C for 1 h. XPS measurements were carried out on a Kratos AXIS Ultra DLD (monochromatic Al Kα), and depth profiling was achieved by sputtering the film with 4 keV Ar^+. X-ray diffraction patterns were collected on a BrukerNonius D8 ADVANCE diffractometer. Film thicknesses were determined using cross-sectional SEM (Hitachi S-5500 and FEI Quanta 650).

Single crystal X-ray crystallography

Suitable crystals were covered in mineral oil and mounted on a nylon thread loop. Crystallographic data were collected on either a Nonius Kappa CCD diffractometer using a graphite monochromator with MoKα radiation (λ = 0.71073 Å) at reduced temperature using an Oxford Cryostream low temperature device or a Rigaku AFC12 diffractometer with a Saturn 724+ CCD using a graphite monochromator with MoKα radiation at reduced temperature using a RigakuXStream low temperature device. Data reduction was performed with either DENZO-SMN or Rigaku Americas Corporation's Crystal Clear version 1.40. All structures were solved by direct methods using SIR2004 and refined by full-matrix least squares on F^2 with anisotropic displacement parameters for the non-H atoms using SHELXL-97. Hydrogen atoms on carbon were calculated in idealized positions with isotropic displacement parameters set to 1.2 × U_{eq} of the attached atom (1.5 × U_{eq} for methyl hydrogen atoms). The function $\Sigma w(|F_o|^2-|F_c|^2)^2$, was minimized, where $w = 1/[(\sigma(F_o))^2 + (0.0528*P)^2 + (0.685*P)]$ and $P = (|F_o|^2 + 2|F_c|^2)/3$. Neutral atom scattering factors and values used to calculate the linear absorption coefficient are from the International Tables for X-ray Crystallography. All figures were generated using SHELXTL/PC.

Details of crystal data, data collection, and structure refinements are listed in Table 2.

Acknowledgements

The authors would like to thank the Welch Foundation (Grant F-816) and the Petroleum Research Fund, administered by the American Chemical Society (47014-ACS) for financial support. X-Ray data were collected on instrumentation purchased with funds from NSF grant #0741973.

References

1 (*a*) A. A. Istratov, C. Flink, H. Hieslmair and E. R. Weber, *Phys. Rev. Lett.*, 1998, **81**, 1243; (*b*) J. D. McBrayer, R. M. Swanson and T. W. Sigmon, *J. Electrochem. Soc.*, 1986, **133**, 1242; (*c*) Y. Shacham-Diamand, A. Dedhia, D. Hoffstetter and W. G. Oldham, *J. Electrochem. Soc.*, 1993, **140**, 2427; (*d*) F. Lanckmans and K. Maex, *Microelectron. Eng.*, 2002, **60**, 125.
2 (*a*) C.-H. Han, K.-N. Cho, J.-E. Oh, S.-H. Paek, C.-S. Park, S.-I. Lee, M.-Y. Lee and J. G. Lee, *Jpn. J. Appl. Phys., Part 1*, 1998, **37**, 2646; (*b*) J. Lin and C. Lee, *J. Electrochem. Soc.*, 1999, **146**, 3466.
3 M. S. Mudholkar and L. T. Thompson, *J. Appl. Phys.*, 1995, **77**, 5138.
4 (*a*) R. Fix, R. G. Gordon and D. M. Hoffman, *Thin Solid Films*, 1996, **288**, 116; (*b*) S. L. Roberson, D. Finello and R. F. Davis, *Thin Solid Films*, 1998, **324**, 30.
5 M. Damayanti, T. Sritharan, Z. H. Gan, S. G. Mhaisalkar, N. Jiang and L. Chan, *J. Electrochem. Soc.*, 2006, **153**, J41.
6 (*a*) J.-H. Shin, A. Waheed, K. Agapiou, W. A. Winkenwerder, H.-W. Kim, R. A. Jones, G. S. Hwang and J. G. Ekerdt, *J. Am. Chem. Soc.*, 2006, **128**, 16510; (*b*) J.-H. Shin, A. Waheed, W. A. Winkenwerder, H.-W. Kim, K. Agapiou, R. A. Jones, G. S. Hwang and J. G. Ekerdt, *Thin Solid Films*, 2007, **515**, 5298; (*c*) J.-H. Shin, H.-W. Kim, K. Agapiou, R. A. Jones, G. S. Hwang and J. G. Ekerdt, *J. Vac. Sci. Technol., A*, 2008, **26**, 974.
7 Y.-X. Li, O. Koper, M. Atteya and K. J. Klabunde, *Chem. Mater.*, 1992, **4**, 323.
8 (*a*) P. Meakin, E. L. Muetterties and J. P. Jesson, *J. Am. Chem. Soc.*, 1973, **95**, 75; (*b*) D. H. Gerlach, W. G. Peet and E. L. Muetterties, *J. Am. Chem. Soc.*, 1972, **94**, 4545.
9 (*a*) K. G. Frank and J. P. Selegue, *Acta Crystallogr., Sect. C: Cryst. Struct. Commun.*, 1991, **C47**, 35; (*b*) G. Albertin, S. Antoniutti, E. Bordignon, G. Pelizzi and F. Vitali, *J. Organomet. Chem.*, 1988, **353**, 229; (*c*) T. Koyama, Y. Koide and K. Matsumoto, *Inorg. Chem.*, 1999, **38**, 3241.
10 (*a*) L. C. Feldman and J. W. Mayer, *Fundamentals of Surface and Thin Film Analysis*, North Holland, New York, 1986; (*b*) H. Y. H. Chan, C. G. Takoudis and M. J. Weaver, *J. Catal.*, 1997, **172**, 336.
11 J. H. Rivers, L. J. DePue Anderson, C. M. N. Starr and R. A. Jones, *Dalton Trans.*, 2012, **41**, 5401.
12 (*a*) G. S. Sandhu, *Thin Solid Films*, 1998, **320**, 1; (*b*) T. Aoyama, M. Kiyotoshi, S. Yamazaki and K. Eguchi, *Jpn. J. Appl.Phys.*, 1999, **38**, 2194; (*c*) E.-S. Choi, J.-C. Lee, J.-S. Hwang, J.-B. Park and S.-G. Yoon, *J. Electrochem. Soc.*, 1999, **146**, 4189; (*d*) Y. Matsui, M. Hiratani, T. Nabatame, Y. Shimamoto and S. Kimura, *Electrochem. Solid-State Lett.*, 2001, **4**, C9.
13 (*a*) P. Scherrer, *Zsigmondy's Kolloidchemie*, Verlag, Berlin, 3rd edn, 1920; (*b*) B. E. Warren, *X-Ray Diffraction*, Dover Publications, Mineola, 1990.